Available online at www.sciencedirect.com
SCIENCE DIRECT®
Continental Shelf Research 25 (2005) 2410–2427
CONTINENTAL SHELF RESEARCH
www.elsevier.com/locate/csr

Fine-grained sediment dynamics during a strong storm event in the inner-shelf of the Gulf of Lion (NW Mediterranean)

B. Ferré[a,*], K. Guizien[b], X. Durrieu de Madron[a], A. Palanques[c], J. Guillén[c], A. Grémare[b]

[a]*Centre de Formation et de Recherche sur l'Environnement Marin, UMR 5110, CNRS—Université de Perpignan, 52 Avenue de Villeneuve, 66860 Perpignan Cedex, France*
[b]*Observatoire Océanologique de Banyuls, Laboratoire d'Océanographie Biologique, UMR 7621, CNRS-UPMC, 66651 Banyuls-sur-Mer Cedex, France*
[c]*Institut de Ciències del Mar, CMIMA—CSIC, Passeig Maritim de la Barceloneta, 37-49, 08003 Barcelona, Spain*

Available online 10 October 2005

Abstract

A 1-month survey, comprising moored instruments and high-frequency sampling, was carried out in a shallow Mediterranean embayment during the autumn of 1999, to assess the effect of strong and unpredictable meteorological events on the near-bed, fine-grained sediment dynamics. A 1DV Reynolds Averaged Navier–Stokes (RANS) model for the wave-current boundary layer [Guizien et al., 2003. 1DV bottom boundary layer modeling under combined wave and current: turbulent separation and phase lag effects. Journal of Geophysical Research 108(C1), 3016] is tested, against the recorded suspended sediment concentration data (SSC); it is used then to determine the sediment resuspension and flux in the embayment.

A strong southeasterly storm occurred on November 12, 1999, which generated a large swell ($H_s = 7$ m, $T_m = 10$ s), a sea surface rise of about 0.5 m and near-bottom currents of up to 35 cm s^{-1}. During the storm, the SSC increased throughout the whole of the water column and reached 70 mg l^{-1}, at 25.8 m (0.5 m above the bottom). Numerical computations of SSC profiles, based upon local sandy sediment grain size distribution, are in good agreement with the measured SSC profiles during the onset of the storm over the first 2 h. These observations confirm that the measured SSC profiles, during the storm, resulted from the resuspension of the fine-grained fraction (<60 μm); that is consistent with the grain size of material collected in sediment traps. Following the first 2 h, numerical simulations suggest that bed armouring occurred, after the surficial fine-grained fraction was winnowed. Computations of mud fraction SSC, along a cross-shore transect, which displays a seaward-fining texture of the sediment, indicate that strong resuspension during this severe storm event only affected water depths shallower than 35 m. This water depth coincides approximately with the transition from sand to mud, on the Gulf of Lion shelf, which is located around 30 m. Computations of the horizontal flux of suspended sediment flux, due to the current alone, agree with the observations; these indicate that the flux integrated, over the bottom 4.1 m above the seabed, during the storm (14 300 kg m^{-2}) is associated mainly with the fine-grained sediment fraction. The fine-grained fraction flux is at least 2.5 times larger than the coarser fractions flux. Likewise, whilst most of the coarse grained flux (99%) is confined within few tens of centimetres above the bottom, more than half of the fine-grained flux occurs above the bottom boundary layer.

Keywords: Fine-grained sediment dynamics; Resuspension modelling; Storm; Gulf of Lion; Mediterranean Sea

*Corresponding author. Fax: +33 4 68 66 20 96.
E-mail address: ferre@univ-perp.fr (B. Ferré).

0278-4343/$ - see front matter © 2005 Elsevier Ltd. All rights reserved.
doi:10.1016/j.csr.2005.08.017

1. Introduction

Due to the oligotrophic character of the Mediterranean waters, resuspension processes are expected to play a key role in the carbon, nutrients and pollutants recycling in the coastal ecosystems. Given that organic matter and pollutants are adsorbed mainly onto fine particles (clays and silts, whose size is smaller than 63 μm), the understanding of the resuspension and transport of fine-grained sediment is a prerequisite to apprehend their dissemination.

The Mediterranean Sea is a micro-tidal and low-energy system. Sediment resuspension is caused primarily by the wave-storm activity. Guillén et al. (2002) and Palanques et al. (2002) showed that sediment resuspension, in response to average waves on the Ebro margin (NW Mediterranean) is only effective on the inner shelf. Further, Puig et al. (2001) have suggested that strong northeastern wave-storm ($H_s > 4.5$ m and $T_s > 11$ s) could resuspend fine-grained sediment from the mid-shelf mud-belt, at 60 m depth. Thus, the setting of the Mediterranean margins is significantly different from shelves affected by strong tidal currents and/or "swell" waves, such as the US eastern and western coasts (Lyne et al., 1990; Madsen et al., 1994; Wiberg et al., 1994; Gardner et al., 2001; Chang and Dickey, 2001), where high-intensity sediment resuspension processes can occur across the entire shelf.

River flooding and energetic storm waves dominate also sediment transport in the Gulf of Lion, north of the Ebro margin. The main attributes of the modern sedimentation in the Gulf of Lion are a mid-shelf mud band and fine-grained deposits on the upper slope, with regions of the inner and outer-shelf dominated by sand (Fig. 1a). Jago and Barusseau (1981) have suggested already that the wave regime is responsible of the seaward transition from sand to mud at water depths around 20–30 m. Indeed, according to the Météo-France wave forecast model VAGMED, swells coming from the SE have a peak period of 6.6 s, on average, over the 1996–2000 period; this locates the inner shelf limit at 34 m (deep-water wave limit). However, over the same period, three storms of strong amplitude (i.e. $H_s > 5$ m, $T_m > 10$ s, with a deep-water wave limit deeper than 78 m) occurred in December 1997, November 1999 and December 2000. The effect of such storms has never been documented in this zone, in particular in relation to processes affecting fine-grained sediment resuspension on the inner shelf. The present study shows the effect of the November 1999 event on the resuspension and dispersal of fine-grained sediment, at a water depth of ~26 m (inner-shelf) off the southwestern coast of the Gulf of Lions (Fig. 1b).

During such strong storms, intra-wave processes are expected to play a significant role; consequently steady models used in most field studies (e.g. Grant–Madsen–Glenn model in Wright et al., 1999; Lee et al., 2002) may fail to predict appropriately the sediment transport. Recently, Storlazzi and Jaffe (2002) showed that steady models break down to estimate both the wave-averaged concentration and the transport of fine sand close to the bed (18 cm a.b.) during energetic wave events by 12 m deep on the inner shelf of central California. These investigations suggested that unsteady models should be more appropriate to account for the instantaneous coupling between fluid flow and sediment suspension. Hence, to overcome this limitation, we use a one-dimensional vertical (1DV) unsteady model, to hindcast suspended sediment concentration (SSC) and transport of the sand and fine-grained sediment within the bottom boundary layer.

In this paper, observations of fine-grained sediment transport in the Gulf of Lion inner shelf are compared to the output from the 1DV oscillatory turbulent boundary layer model of Guizien et al. (2003). After describing the hydrodynamic and hydrological measurements collected with instrumented mooring lines, at a water depth of ~26 m over a 1.5 month period, the SSC data are compared to SSC computations derived using the 1DV unsteady model. Following validation, the time-varying model is used further to assess the impact of the storm on the remobilisation of the local sediments and horizontal sediment transport. Finally, larger-scale inferences, related to how strong storms would control the sand–mud transition, are made.

2. Material and methods

2.1. Measurement site

The Bay of Banyuls is a small embayment located at the southwestern tip of the Gulf of Lions (Fig. 1b); it is bordered to the north by the Béar Cape, a promontory that partly protects the bay, from the predominant northwestern continental wind (Tramontane). The Têt River, located 20 km

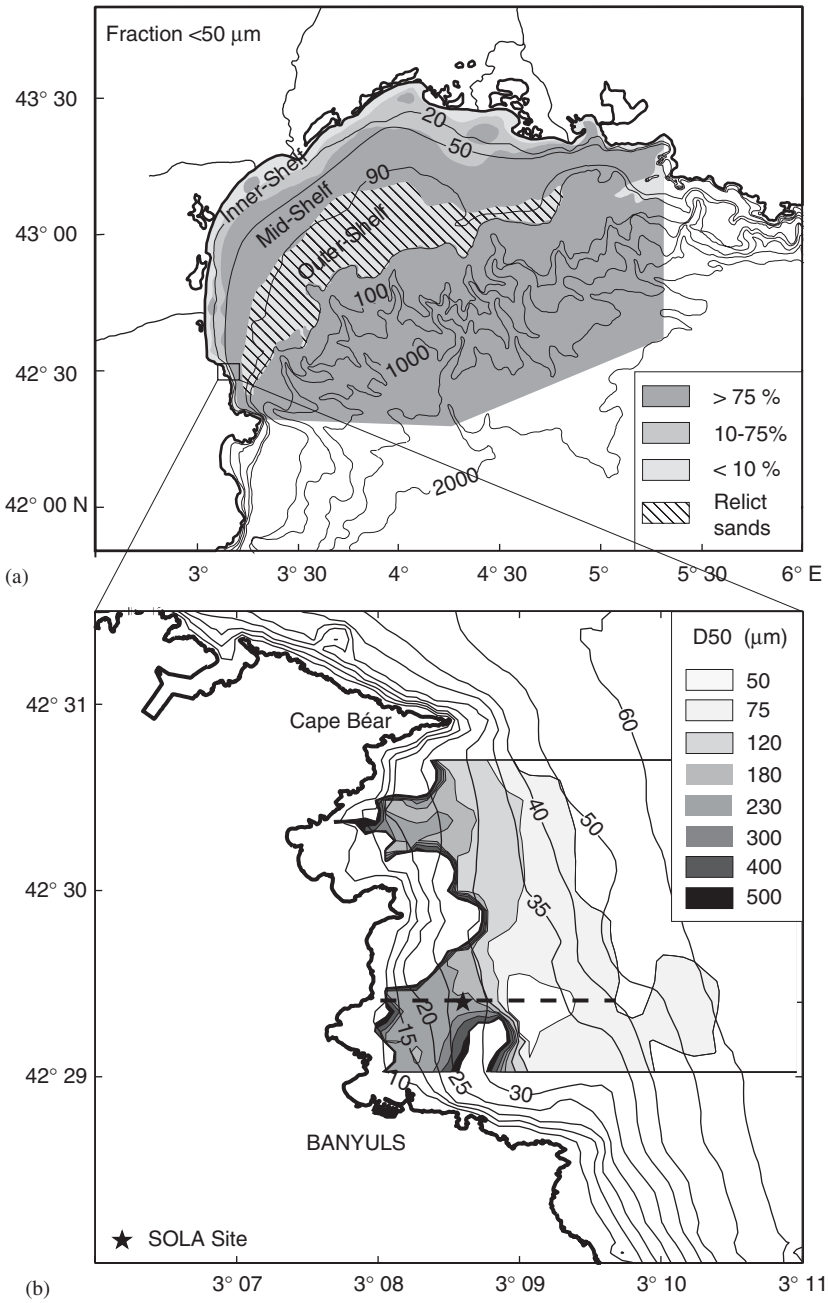

Fig. 1. Bathymetry and sediment grain size distribution in the Gulf of Lion (a) and the Bay of Banyuls (b) at the southwestern tip of the gulf. The location of the mooring array (SOLA site) at a depth of 26.3 m is indicated. The dashed line represents the cross-shore transect, as used in the text.

north of the bay, is the main river supplying freshwater in the area.

The bottom sediments of the bay are composed mostly, between 6 and 30 m water depth, of well-sorted fine sand; deeper than 30 m, of mud (Fig. 1b). At the Service d'Observation du Laboratoire Arago (SOLA) site, located in the southern part of the bay at a 26.3 m water depth, the sediment is composed of fine sands. Moreover, with an organic carbon content of 0.2% and a total carbon content less than

4%, the sediment is mostly terrigenous in origin. The proportion of the main grain size classes is listed in Table 1.

Wave characteristics from the southwestern part of the Gulf of Lions were estimated from the outputs of the Météo-France wave-forecast model, VAGMED. The analysis of the data compiled every 6 h during the 1996–2000 period (Fig. 2), indicates that waves have, on average, a significant height and mean period of 1.2 m and 4.8 s, respectively. Two incoming wave directions predominate: short waves, generated by Tramontane wind coming from the northwest (average mean period of 5.7 s); and swells associated to southeasterly winds (average mean period of 6.6 s). The largest swells, with periods up to 12 s, always originate from E–SE, then occur between late autumn and early spring.

Table 1
Grain size classes of the sediment at the SOLA site (see Fig. 1) defined by their percentage, median grain size and corresponding settling velocity

Size range	% of each grain size class	Settling velocity ($cm\,s^{-1}$)	Corresponding D_{50} (μm)
Silt and clays, 0–60 μm	5.2	0.08	30
Fine sand, 60–120 μm	10.9	0.89	106
Medium sand, 120–239 μm	42.2	2.46	191
Coarse sand, >239 μm	41.7	5.90	388

2.2. Instruments and data collection

The experiment began on October 29, 1999 and ended on December 04, 1999. Four moorings were deployed, side-by-side, next to the SOLA site (Fig. 3). A non-directional WaveRider buoy measured free surface elevation, during a 20 min burst every 30 min. From buoy surface elevation measurements, wave height and period maximum, significant height and

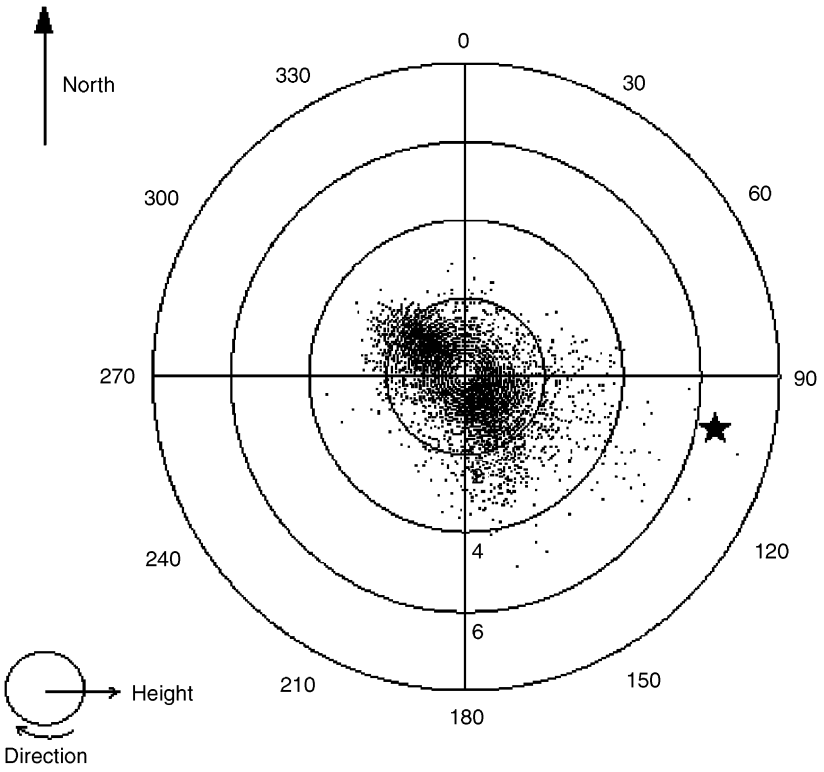

Fig. 2. Significant wave height and direction in the western part of the Gulf of Lions (43°N; 03°30′E), from 1996 to 2000 (6 hourly data from the VAGMED wave prediction model of Météo-France). The radius represents the height (in metres) and the incoming direction of the waves is represented by degrees. The star indicates the height and incoming direction of the waves during the November 12, 1999 storm. Waves higher than 6 m represent 0.09% of the 1996–2000 data, whilst waves originating from the southeast represent 37% of the data.

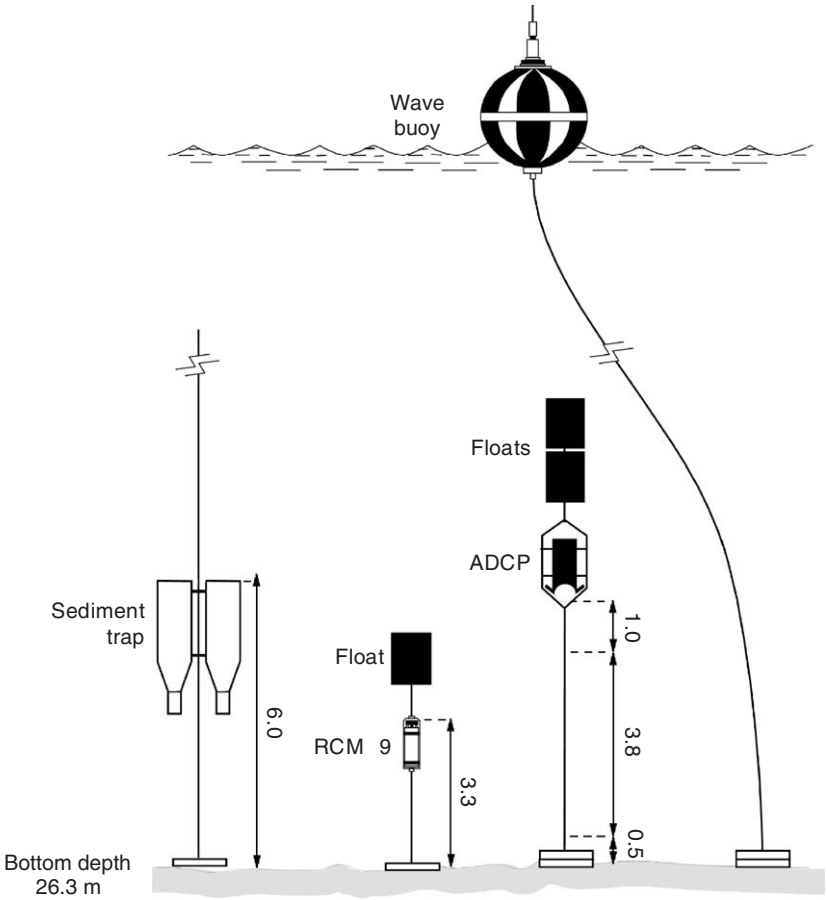

Fig. 3. Schematic of the wave buoy, RCM9 and ADCP and sediment trap moorings. The RCM9 was 3.3 m a.b., the ADCP was 5.3 m a.b and the sediment trap was 6.0 m a.b. The wave buoy measured the surface elevation.

period, and spectral density (from 0.04 to 0.6 Hz) were derived.

The second mooring was equipped with an Aanderaa Doppler current metre (RCM9), located 3.3 m a.b. (metres above bottom). This instrument measures pressure, temperature, turbidity, current speed and direction. Turbidity sensors were Aanderaa Optical Backscatter Sensor (OBS) with two different sensitivity ranges (0–5 NTU and 0–20 NTU, NTU: Nephelometric Turbidity Unit). The sampling rate was set to 5 min.

The third mooring was equipped with a downward-looking RDI broadband 300 kHz ADCP, located 5.3 m a.b. Current velocity and backscattered acoustic intensity were sampled over 30 bins; the bin length was 0.2 m (shallow water mode). This mode uses a pulse-to-pulse coherent processing and works in shallow water, with high water velocity. Due to reduced range and near-bottom corruption of the echo return, between the main and the side lobes, the first valid cell was 4.1 m a.b and the last was 0.5 m a.b. The recorded data consist of burst samples of 100 pings, averaged over 2 min every 15 min. During measurements, the ADCP is able to provide information about the percentage of good-recorded values. Missing values observed in Fig. 4g are due to the low percentage of good values.

An additional mooring, with sediment traps at 6.3 m a.b and 16.3 m a.b, was deployed nearby; its sample cup was recovered and replaced every 3 or 4 days. The material collected by the bottommost trap was used also to define the characteristics of the settling particles.

Profiles of temperature, salinity and turbidity, from the surface down to few metres (2–3 m) above bottom were performed using a self-contained SBE 19 CTD probe, with a 0.25 m Seatech light-transmissometer. Profiles were obtained daily, when

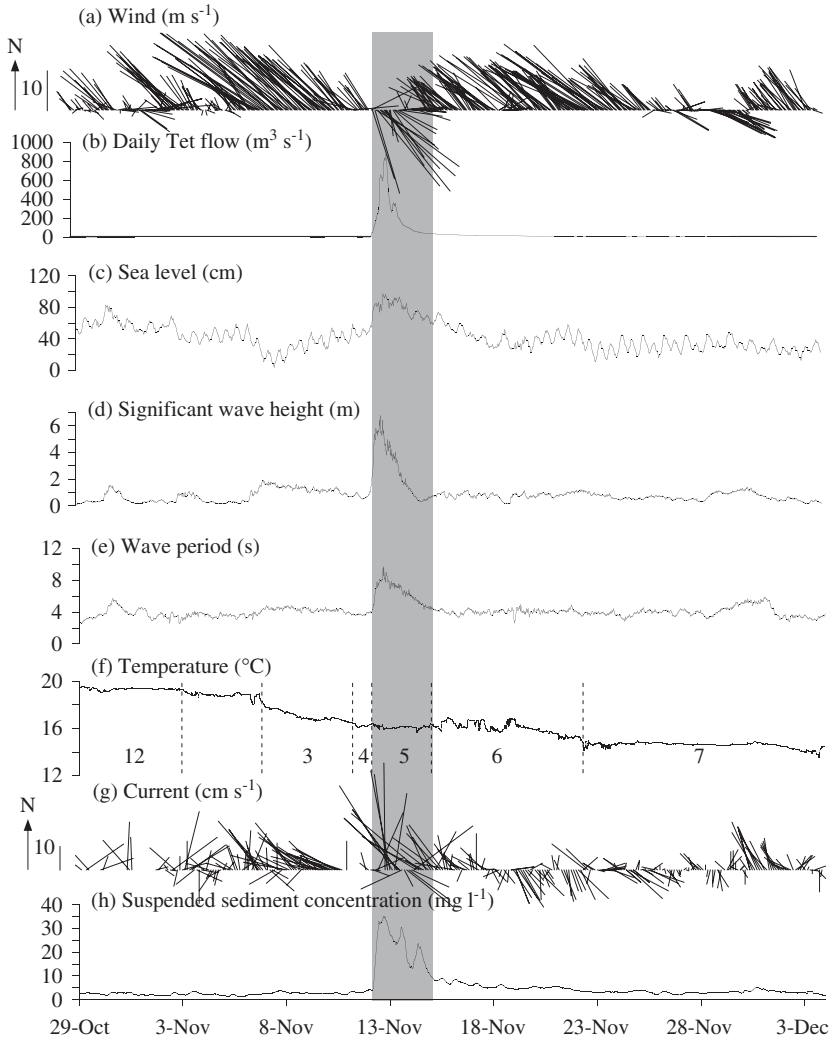

Fig. 4. Time-series of wind velocity, river discharge, sea level, wave characteristics (height and period), temperature, current and SSC at 3.3 m a.b. from ADCP, from October 29th to December 3th, 1999. Wind sticks represent the direction from which the wind is blowing, whereas current sticks represent the direction towards which the current is flowing. The latter results are detailed in Fig. 9. Shaded area delimits the storm period. Periods taken into account for the conversion of backscatter intensity to SSC, delimited by 1 °C or hydrodynamic changes, are delimited by dashed lines.

the sea state allowed it; a total of 25 profiles were realized, during the period of the experiment.

Water samples were taken simultaneously at 19.3, 11.3, 4.3, 3.3 m a.b. and near the bottom with 121 Niskin bottles, for geochemical analysis. The sample at 3.3 m a.b. was located next to the RCM9. SSC was measured gravimetrically from water samples. Volumes of water were filtered through pre-weighted membranes (GF/F Whatman glass fibre, 0.7 μm mean pore size). After drying, their weight increase yielded particulate matter concentrations. The size distribution of individual particles collected in sediment traps, suspended sediment and sediment samples was measured using a Malvern Mastersizer 2000.

Hourly averaged wind speed and direction were measured by Météo-France, at Cape Béar meteorological station (3 km north of the experimental site). Sea level was measured by the *Service Maritime et de Navigation du Languedoc-Roussillon* at Sète, about 100 km north of Banyuls. Daily river discharge of the Têt River was measured by the *Direction Départementale de l'Équipement*.

2.3. SSC data analysis

2.3.1. Calibration of CTD transmissometer

The Seatech light transmissometer measures the transmitted intensity (T in percent), of a 660 nm monochromatic wave along a fixed optical path ($L = 0.25$ m). The attenuation coefficient (c in m^{-1}), due to absorption and diffusion by both water and suspended particles, is derived from the transmission with the equation:

$$c = -(1/L)\,\mathrm{Ln}\,(T). \quad (1)$$

Using data from water samples collected in different coastal areas of the northwestern Mediterranean, Guillén et al. (2000) derived a linear relationship between the attenuation coefficient and SSC (expressed in mg l^{-1}):

$$\mathrm{SSC} = 1.43 \times c - 0.26 \quad (r^2 = 0.85, n = 569). \quad (2)$$

2.3.2. Calibration of OBS

OBS measures the intensity of the light backscattered by particles. The signal is calibrated with a nephelometric solution and is expressed in NTU. Using the gravimetric measurements of SSC carried out on water sampled next to the RCM9, Guillén et al. (2000) related the turbidity to the SSC (expressed in mg l^{-1}) in the water, with the equation:

$$\mathrm{SSC} = 1.21 \times \mathrm{NTU} + 0.43 \quad (r^2 = 0.46, n = 25). \quad (3)$$

2.3.3. ADCP backscattered intensity

SSC were derived from backscattered acoustic intensity, with the commercial Sediview software (Land and Bray, 2000), using the sonar equation:

$$\mathrm{EL} = \mathrm{SL} - 2\mathrm{TL} + \mathrm{TS}, \quad (4)$$

where EL and SL are the echo and source levels, respectively (in dB). TL is the transmission loss and is equal to $20\log_{10}(R) + (\alpha_w + \alpha_s)R$, where α_w and α_s are the absorption coefficients by water and sediment, respectively and R is the distance from the transducer to the depth cells. TS is the target strength and is related to the mean acoustic cross-section of the scatterers $\sigma = N\sigma_s$, where N is the particle density and σ_s is the individual acoustic cross-section, within an insonified volume V. If the SSC (in kg m^{-3}) is $N\rho_s\upsilon_s$, where ρ_s is the density and υ_s is the volume, TS is equal to $10\log_{10}$ (SSC $\sigma_s/\rho_s\upsilon_s$) $+ 10\log_{10}(V)$.

The sonar equation then reads:

$$\mathrm{EL} = \mathrm{SL} - 40\log_{10}(R) - 2R(\alpha_w + \alpha_s) + 10\log_{10}(\mathrm{SSC}\ \sigma_s/\rho_s\upsilon_s) + 10\log_{10}(V). \quad (5)$$

Defining the relative backscatter intensity, measured by the ADCP and corrected from beam spherical spreading, as

$$N(R) = \mathrm{EL} - \mathrm{SL} + 40\log_{10}(R). \quad (6)$$

Thus, the SSC can be expressed as

$$10\log_{10}(\mathrm{SSC}) = N(R) + 2R(\alpha_w + \alpha_s) - 10\log_{10}(\sigma_s/\rho_s\upsilon_s) - 10\log_{10}(V) \quad (7)$$

or equivalently

$$\log_{10}(\mathrm{SSC}) = [N(R) + 2R(\alpha_w + \alpha_s) + \mathrm{Ks}]/S, \quad (8)$$

where $\mathrm{Ks} = -10\log_{10}(\sigma_s/\rho_s\upsilon_s) - 10\log_{10}(V)$ and $S = 10$.

Theoretically, S has a value of 10, but it is allowed to vary in the Sediview method, in order to fit the backscattered intensity with the measured SSC.

The coherence of the backscatter data from the four beams was checked and the outliers were removed, before averaging. The temperature record at 3.3 m a.b. showed strong temporal variation during the course of the experiment (Fig. 4f). Therefore, seven periods were identified for the calibration. For each period, the median size (D_{50}) was derived from the grain size analysis undertaken on the sediment traps samples. The calibration constants S and Ks were then determined, by fitting by least square sense, the ADCP measurements with the water samples, except during the storm when no water samples were available. During this period, we relied upon unsaturated OBS measurements (0–20 NTU range). Values of the calibration parameters are reported in Table 2. The relative backscatter coefficient S appeared to be constant and equal to 25, throughout all the periods. In contrast, the site and instrument parameter Ks varied during the experiment, ranging between 42 and 52 dB, with the larger values prior to the storm. These variations did not appear to be related to temperature and salinity variations. Ks was fairly constant for the first three periods (Ks = 49−52 dB), whilst the temperature decreased by about 3 degrees; it decreased whilst temperature and salinity were nearly constant. Ks was affected possibly by the presence of biological particles, during the first three periods. Indeed, Grémare et al.

Table 2
Physical properties and parameters values used to calibrate the ADCP signal, for the different periods presented in Fig. 4

Period	29 Oct.–03 Nov.	03 Nov.–07 Nov.	07 Nov.–11 Nov.	11 Nov–12 Nov.	12 Nov.–15 Nov.	15 Nov.–22 Nov.	22 Nov.–03 Dec.
Temperature (°C)	19.4	18.9	17.0	16.4	16.0	15.9	14.6
Salinity (psu)	38.2	37.2	37.4	37.7	37.4	37.5	37.9
Ks (dB)	49	52	51	47	42	43	46
S	25	25	25	25	25	25	25

(2003) showed the presence of a phytoplanktonic bloom, with a large integrated chlorophyll *a* concentration at the end of the first period ($80\,mg\,m^{-2}$). Chlorophyll *a* concentration remained high during the second period ($50\,mg\,m^{-2}$); it decreases progressively until the storm ($20\,mg\,m^{-2}$). After the storm, chlorophyll *a* concentrations remained low ($20\,mg\,m^{-2}$). The covariance of the parameter Ks, with the chlorophyll *a* concentration, may be explained by a modification of the back-scattered signal due to a higher content of organic matter, for similar SSC values.

2.4. 1DV time-varying model

The 1DV time-varying Reynolds averaged Navier–Stokes (RANS) model is based upon the k–ω turbulent model, for oscillatory flow plus current by Guizien et al. (2003); in this, turbulence damping by stratification is taken into account in a linearized form ($\Omega = 0$). Basically, this turbulence model is similar to the Wilcox transitional k–ω model (1992), in which diffusion and transition constants have been modified to agree best with direct numerical simulations and experimental results, for time-varying oscillatory flows.

Recently, it has been shown by Storlazzi and Jaffe (2002) that steady sediment transport models, based upon the product of the wave-averaged current and SSC profile, failed to predict both the wave-averaged concentration and the transport of fine sand close to the bed (18 cm a.b.) during energetic wave events by 12 m depth. Storlazzi and Jaffe (2002) explained that steady models fail, due to the lack of information regarding the instantaneous coupling between fluid flow and sediment suspension. We emphasize here that this instantaneous coupling not only means the wave-transport resulting from the average of concentration and velocity fluctuations, but affects also the wave-averaged SSC profiles through the instantaneous sediment stratification feedback on the flow. Regarding fine-grained sediment, which hardly settles out, the sediment concentration shows only time-variations very close to the bed. However, such time-variations in the sediment stratification are likely to affect the wave-averaged SSC profiles through instantaneous feedback on turbulence. This unsteady model, including turbulence damping by the sediment density stratification, should overcome this latter failure mode of steady models. In addition, it enables the near-bed sediment transport to be hindcasted, although this was not measured.

The turbulent model forcing conditions are the velocity outside the wave boundary layer, throughout a wave period, and the bottom roughness. The computational grid is exponential, with a near-bed step size of 10^{-6} m and 220 points over 6.15 m. Velocity outside the wave boundary layer is prescribed, at 6.15 m a.b., as the sum of a constant velocity (current) and a time-varying sine velocity; its amplitude and period are derived from the wave characteristics (significant height and mean period), by applying the linear wave theory for a given water depth. This assumption is supported by the symmetry of the free surface elevation records, during the storm (data not shown). To derive the angle between current and waves, we assume that waves were coming from the east, as suggested by VAGMED data statistics. Hydrodynamic conditions encountered during the onset of the storm, as used for SSC simulations, are given in Table 3. Bottom roughness is the Nikuradse roughness, based upon the local median grain size. It should be noted that using a 1DV model rely upon the assumption that the bedforms are washed out, which is generally valid during storms (sheet flow conditions, for A4 ab and A5 periods, Table 3). However, the mobility number derived for A1 condition suggests that vortex ripples could have developed.

Time-varying SSC profiles are computed, assuming that the bed sediment is a mixture of four grain size classes, as defined in Table 1. For a given grain

Table 3
Hydrodynamical conditions encountered during the storm at SOLA site (see Fig. 1), defined by the current intensity and wave characteristics

Condition	U_c (cm s^{-1})	T_m (s)	H_s (m)	U_w (cm s^{-1})	Φ (deg)	Ψ mobiliy number relative to $D_{50} = 200\,\mu m$
A1	8	7.3	4.5	50	0	75
A2	6.5	7.7	5.2	67	0	134
A3a	10	7.7	5.2	67	0	134
A3b	12	7.7	5.2	67	0	134
A4a	20	8.1	5.8	83	90	206
A4b	30	8.1	5.8	83	90	206
A5	25	9.7	6.8	128	90	491

U_c is the current velocity, T_m is the mean wave period, H_s is the significant wave height, U_w is the orbital velocity, Φ is the angle between the current and the wave, and Ψ is the mobility number.

size class i, the following time-dependent sediment concentration $C_i(t,z)$ balance is solved:

$$\frac{dC_i}{dt} = \frac{d}{dz}(W_{si}C_i) + \frac{d}{dz}\left(\gamma_t \frac{dC_i}{dz}\right), \quad (9)$$

where t is time, z is the vertical dependent, γ_t is the sediment diffusion (which is set equal to the eddy diffusion computed in a coupled turbulence model), $W_{si} = W_{si0} \times (1 - C_i)^4$ is the sediment hindered settling velocity and a series of boundary conditions are applied (see below):

(a) at $z = 2 \times D_{50\,i}$, with $D_{50\,i}$, the median grain diameter of the grain size class i: $C_i = \max(C_a, C_b)$ where $C_a = K_i \times C_{ref\,i}$ with $C_{ref\,i}$ the reference concentration obtained by applying instantaneously Engelund and Fredsøe's (1976) formula (quasi-steady approximation) for class i, and K_i is the weight proportion of class i in the bed sediment. C_b results from the particles settling from the upper layers. Hence, sediment is allowed to deposit on the seafloor when the settling velocity is larger than the diffusive flux.
(b) at $z = z_h$, zero flux of sediment reads $dC_i/dz = 0$.

The settling velocity at rest W_{si0} is set according to the median grain size diameter of each class, as defined in Table 1. For sand classes, the settling velocity is computed by the Zanke formula (1977) for spherical grains of respective median diameter. All the fine-grained sediment is contained within the 0–60 μm class, with a settling velocity of 0.8 mm s^{-1}. This velocity corresponds to both the Stokes velocity for spherical grains of 30 μm and the settling velocity of fine-grained flocculates of about 200 μm, according to Gibbs (1985). Indeed, local observations by Durrieu de Madron et al. (this volume) have showed than fine particles tend to aggregate into flocs, of about 100–200 μm in size.

Finally, the coupled model (turbulence and concentration) is run for the hydrodynamic conditions given in Table 3, with a bed mixture corresponding to the one measured prior to the storm (Table 1).

3. Results and discussion

3.1. Meteorological, hydrodynamic and hydrological conditions

3.1.1. Wind and wave

The 1996–2000 data from the VAGMED wave-forecast model of Météo-France reveal three strong storms, with significant wave heights and periods greater than 5 m and 10 s, respectively; these occurred on December 17, 1997, November 12, 1999 and December 23, 2000. Thus, the storm under study is a strong annual event. Northwesterly winds (Tramontane) predominated, during the period of the experiment (Fig. 4a). Two long periods of Tramontane, with wind velocities larger than 30 m s^{-1}, lasted from the sixth to the 11th November and from the 16th to the 26th November 1999. Significant wave height and mean period during these periods were about 1 m and 4 s, respectively. Two short events of southeasterly wind occurred on the 12th to the 14th November and the 28th to 30th November. Only the 12–14 November episode was accompanied with strong rains, which caused a flooding of the coastal rivers (e.g. the Têt river, in

Fig. 4b) and a significant rise of the sea level (from 50 cm, on average, to 100 cm, Fig. 4c) due to the low atmospheric pressure (from 1021 hPa, on average, to 1000 hPa) and the shoreward water transport by the wind. During this period, large irregular, but symmetric, swells were observed (Fig. 4d, e); these had significant wave heights and mean periods reaching values of 7 m and 10 s, respectively, on November 12, 1999.

3.1.2. Currents

RCM9 and ADCP current intensity time-series, at 3.3 m a.b., are in good agreement (RMS difference of 1 cm s^{-1}, the statistical precision of both instruments). Current velocity and direction show rapid variations in time (Fig. 4g); these may be explained by fluctuations in local winds and the outer bay circulation, which interacts with the jagged coastline. Before and after the storm, current intensity and direction were rather homogeneous within the near-bottom layer, with a fairly constant speed (~5–10 cm s^{-1}) between 4.3 m a.b. and 0.9 m a.b. During and immediately after the storm (until November 18th), the current was oriented to the N–NW and reached speeds of 35 cm s^{-1}.

3.1.3. Thermohaline properties

Although the last metres of the water column were not sampled, profiles of temperature and salinity (Fig. 5a and b) together with the time-series of temperature at 3.3 m a.b (Fig. 4f) illustrate the temporal evolution of the thermohaline structures within the water column. The water column underwent large changes, due mainly to wind-induced mixing and cooling effects. In early November (November 2), the water column was strongly stratified with a thin surface layer of cold brackish water. After a first strong northwesterly wind (Tramontane) event (November 6–11), the surface layer water was mixed down to the bottom and a cooling of about 2–3 °C was observed in the water column, resulting in a non-stratified water column. After the storm, a layer of warmer and saltier water was observed below 4.3 m a.b., resulting in a little stratification in density that persisted until November 19 (profiles not shown). It is not possible to infer the origin of this warm salty water from single point measurements, due to the high variability in the Banyuls bay circulation. The strong discharge of freshwater from the river, observed in Fig. 4b, did not affect the salinity in the Bay. This observation indicates that there was no impact of terrigenous material transported by the river plume. In late November–early December, another Tramontane episode homogenized the water column, which reached rather low temperature (T~14.5 °C) and high salinity (S~38).

3.2. Suspended particles, sediment fluxes and bottom sediment

Temporal variability of the turbidity series recorded by the OBS and the ADCP were well correlated (Fig. 6b), with a RMS difference of 1.7 mg l^{-1} over the entire period. Profiles of SSC, measured over the entire water column, ranged between 0.5 and 3 mg l^{-1} during "calm" periods (i.e. before and long after the storm), but showed a 2–3 fold increase immediately after the storm (Fig. 5c). ADCP-derived SSCs show an abrupt increase at the onset of the storm, from 2–3 to 25 mg l^{-1} at 4.1 m a.b. (Fig. 6a), from 3–5 to 50 mg l^{-1} at 1.5 m a.b. (Fig. 6c) and from 7 mg l^{-1} to 70 mg l^{-1} closest to the bottom (0.5 m a.b., data not shown). The temporal evolution of the SSC indicates that it took about 8 days after the storm for the system to recover, reaching SSC lower than 5 mg l^{-1} at 3 m a.b.

Measured suspended sediment flux, due to current alone and integrated between 0.9 and 4.1 m a.b., shows an increase from 100 kg m^{-2} (integrated over 15 days) before the storm to 2235 kg m^{-2} during the storm (integrated over 1 day).

The bottom sediment grain size distribution underwent significant changes. Before the storm, the bottom sediment was well-sorted fine sand, showing an unimodal grain size distribution and with a median grain size of 190–200 μm. Immediately after the storm, the fine-grained fraction (<60 μm) increased from 6 to 31%. The bottom sediment grain size distribution was bimodal, with one peak centred at 200 μm and the second at 10 μm. The fine-grained fraction decreased again to 6%, 2 weeks after the storm (unimodal grain size distribution), indicating that the fine-grained fraction was winnowed by the post-storm currents.

3.3. Comparison between observed and predicted SSC profiles

3.3.1. Effect of grain size

Observed SSC profiles were compared with SSC profiles obtained by solving the concentration advection–diffusion equation, presented in

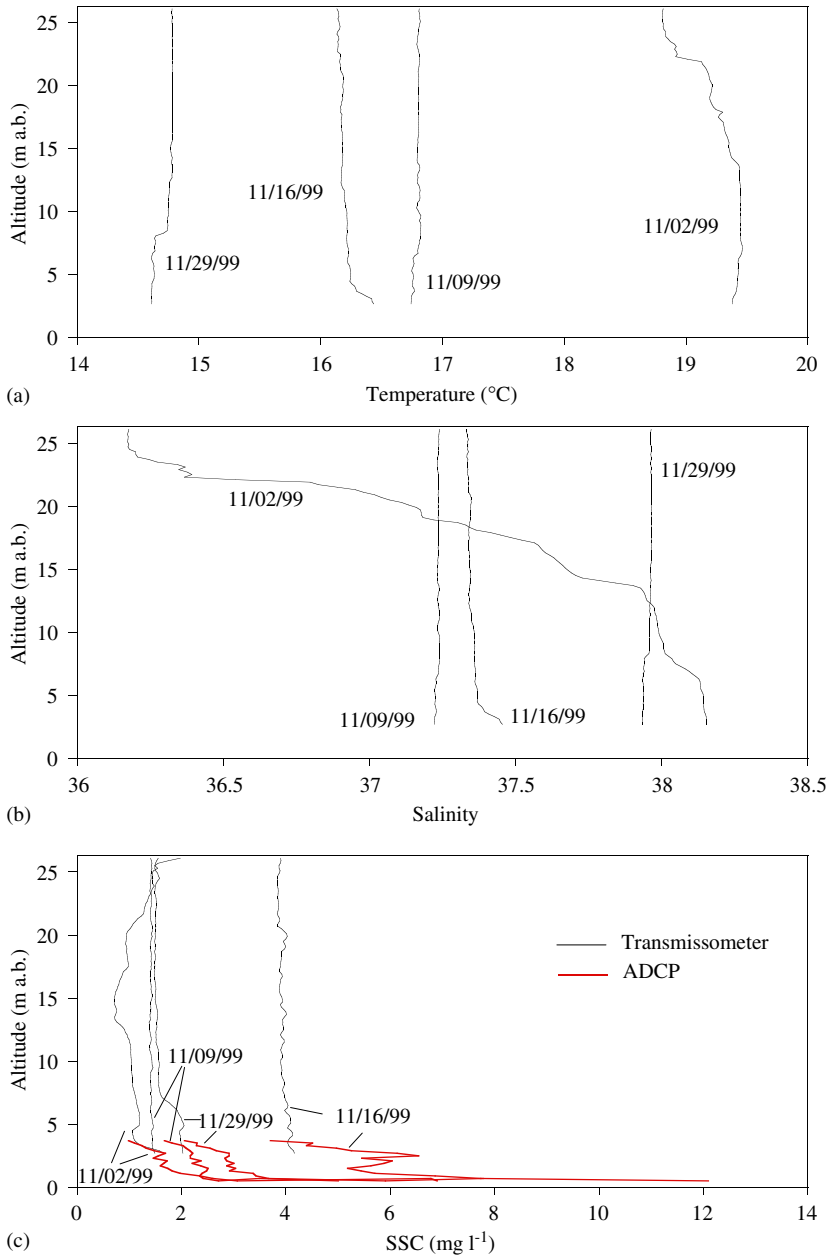

Fig. 5. Vertical profiles of temperature (a), salinity (b) and SSC (c) profiles before (02 and 09 November), immediately after the storm (16 November) and 2 weeks after the storm (29 November). Note: the profiles ended 2–3 m above the bottom.

Section 2.4 and averaged over a wave period. Firstly, the model was used to assess the size characteristics of the suspended sediment. Secondly, data were used to validate quantitatively the model for SSC computations, during the onset of storm (1DV approximation). Finally, the model was used to determine the depth interval in which this storm could induce sediment resuspension.

SSC profiles, according to the four classes defined in Table 1, were computed for hydrodynamic conditions corresponding approximately to the maximum of the storm ($U_w = 1.28\,m\,s^{-1}$, $T_m = 9.7\,s$, $U_c = 0.25\,m\,s^{-1}$, $\varphi = 90^\circ$) and plotted on Fig. 7. The concentration for sediment with a median grain size larger than 60 μm was lower than $3\,mg\,l^{-1}$, between 1 and 4 m a.b.; this means that

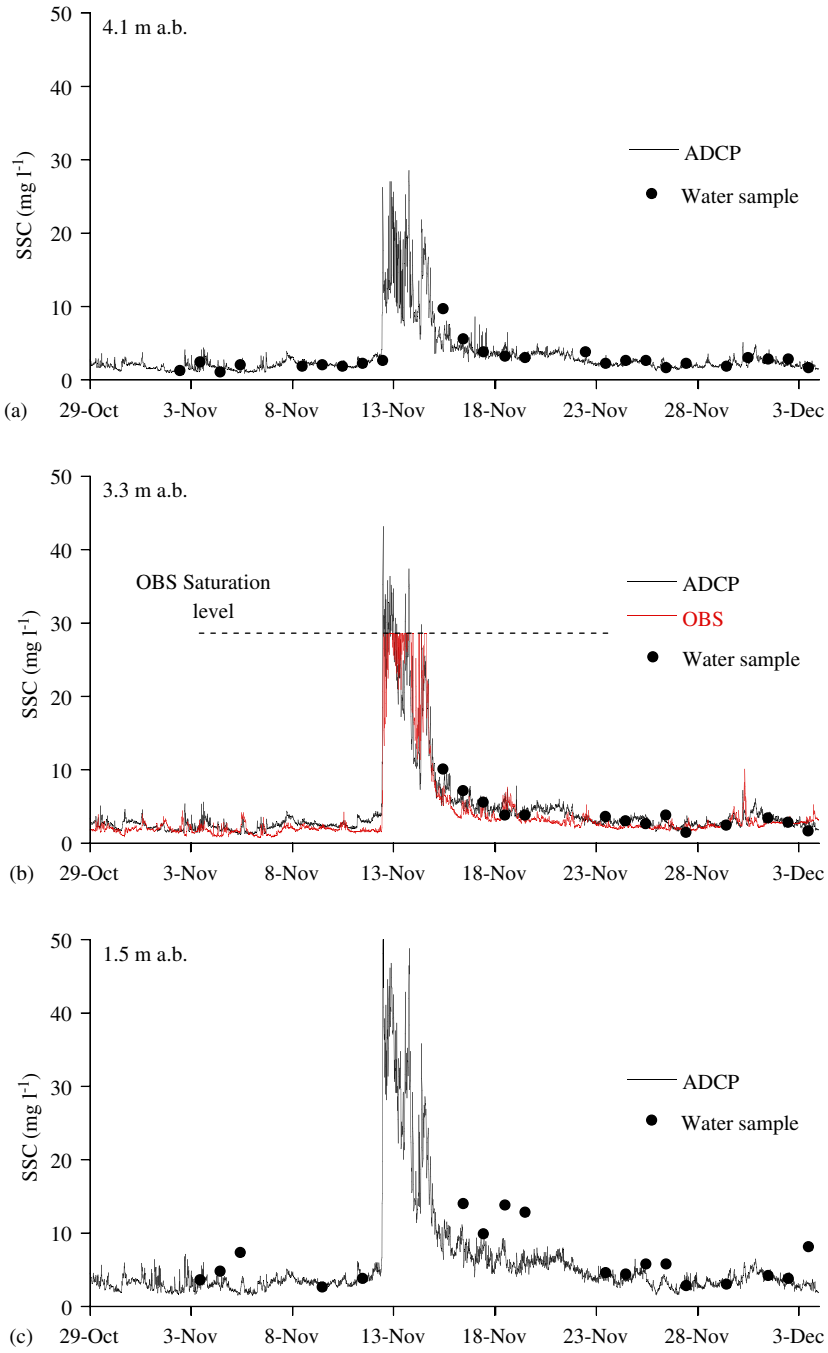

Fig. 6. SSC time-series at 4.1, 3.3 and 1.5 m a.b. derived from ADCP acoustical backscattered intensity and water sample data. The time-series at 3.3 m a.b. included also the OBS-derived SSC.

practically only the fraction finer than 60 μm contributed to the measured SSC (about 20 mg l^{-1}). This observation is confirmed by the relatively small size of the particles collected in the sediment traps, after the storm ($D_{50} = 22$ μm, $D_{90} = 100-125$ μm); these were slightly coarser than the median size of the trapped particles during "calm" periods ($D_{50} = 14$ μm, $D_{90} < 63$ μm).

Hereafter, only SSC profiles for the finest fraction were computed for the various hydrodynamic

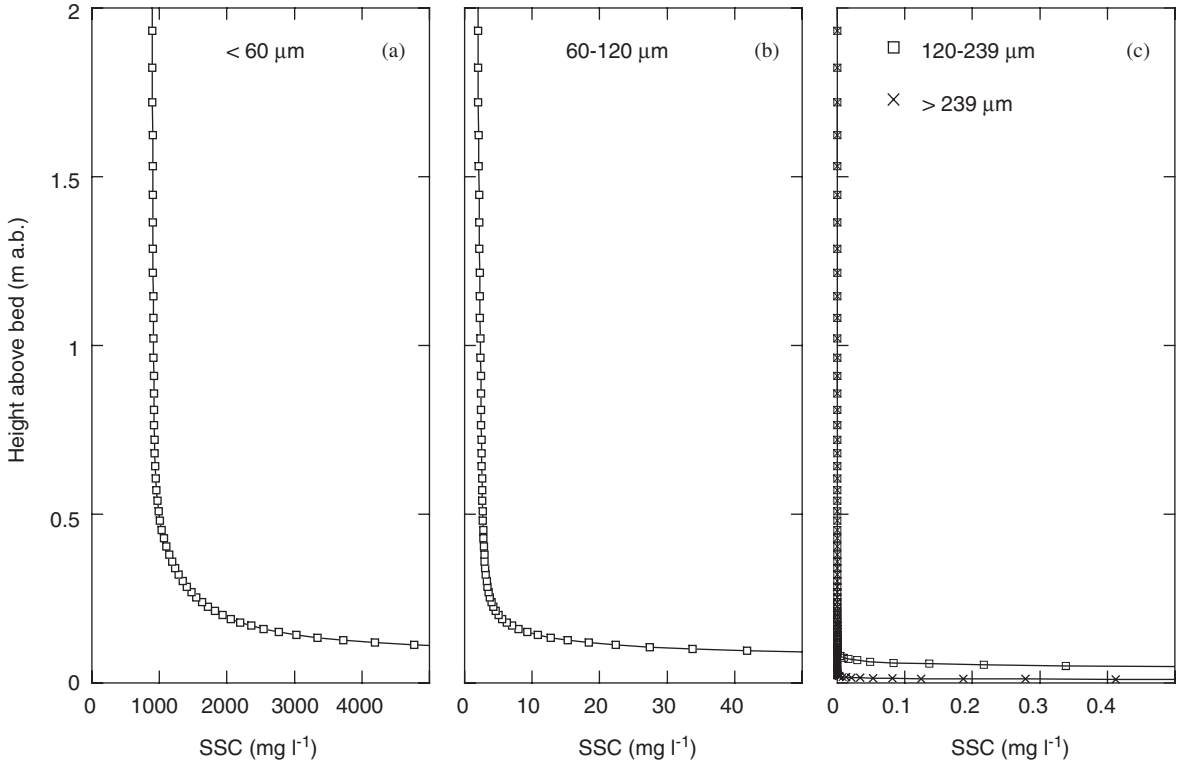

Fig. 7. Computed SSC profiles for four grain size classes: $<60\,\mu m$ (a), 60–120 µm (b), 120–239 µm and larger than 239 µm (c), using hydrodynamic conditions corresponding to the maximum of the storm (A5, $U_w = 128\,cm\,s^{-1}$, $T_m = 9.7\,s$, $U_c = 25\,cm\,s^{-1}$, $\phi = 90^\circ$) and settling velocity given in Table 1. SSC profiles for the two largest classes are close to zero.

conditions prior and during the storm (Table 3). Detail of the hydrodynamic parameters measured during the onset of the storm, between 8 h 50 min and 13 h 50 min on November 12th, is plotted in Fig. 8. These computations have assumed that the particles in suspension derived mainly from the fine fraction of the local bottom sediment. This assumption is supported by the small advection (current velocity lower than $10\,cm\,s^{-1}$), which excludes significant inputs from the muddy zones, during the first hours of the storm.

3.3.2. *Temporal changes during the storm*

The storm period was subdivided in several subperiods defined by different current intensities and wave characteristics (Table 3). Computed and observed SSC profiles are plotted in Fig. 9a, showing very good agreement for the A1–A3 periods (from 8 h 50 min to 11 h 02 min), although the 1DV assumption is not fulfilled at the very beginning of the storm (A1). Indeed, there should be vortex ripples formation, which is not taken into account in this model. We suggest this good agreement is due to the fact that convection only dominates over diffusion near the bed, in the region between the bed and two ripples height (lower than 10 cm).

The discrepancies between the computed SSC profiles and the measurements, during the A4a and A4b periods (Fig. 9b), relate probably to the decrease in the fine-grained fraction availability in the local sediment. Indeed, for these hydrodynamic conditions, the measured SSC profiles were reproduced in the computations, by decreasing the fine-grained fraction down to 0.7% (Fig. 9b). This reduction could result from the coarsening of the sediment and the shielding of fine-grained particles deeper in the bed (bed armouring), after the surficial fine-grained fraction had been resuspended and winnowed by the currents. The strong increase in the current meant also that, from 11 h 32 min on November 12th, the SSC profiles could no longer be modelled with a 1DV approach. Advection became important and the SSC was likely to be dependent upon the exchange of fine-grained particles, with the adjacent zones. On Fig. 9b, we show also SSC

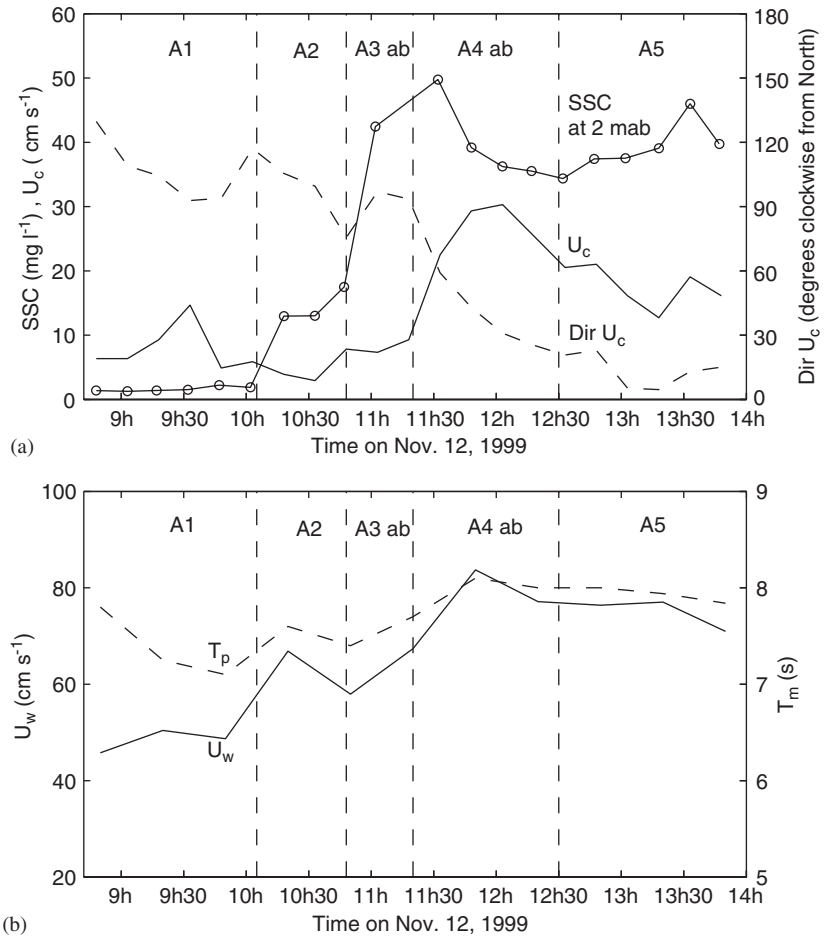

Fig. 8. Detail of hydrodynamic parameters time series and SSC variations at 2 m a.b., measured during the onset of storm. U_c is the current velocity, Dir U_c is the current direction, U_w is the orbital velocity and T_m is the peak period. Characteristics values for each period are summarized in Table 3.

profiles computed with a 100% fine-grained fraction (i.e. no limitation on fine supply); these exhibit the strongest damping effect of stratification, on turbulence. Indeed, for the A4a hydrodynamic condition, SSC computations at 2 m a.b. were similar taking either 5.2 or 100% of fine-grained fraction in the sediment; however, they were still much larger than the measured SSC profiles.

Our observations are coherent with the results of previous studies (e.g. Shi et al., 1985; Drake and Cacchione, 1989; Wiberg et al., 1994) which have shown that the fine-grained fraction, although it comprises only a low percentage of the sandy inner shelf sediments, is more easily resuspended than the coarser fractions and dominates the SSC signal during high stress events. These other investigations have further emphasized the effect of bed armouring, which limits its erodability and reduces the availability of the finer particles, for transport in suspension.

3.3.3. *Suspended sediment flux*

Horizontal suspended sediment transport for the different size fractions, at the study site (26.3 m depth), were computed for the average storm conditions ($U_w = 0.83\,m\,s^{-1}$, $T_m = 8.1\,s$, $U_c = 0.25\,m\,s^{-1}$, $\phi = 90^\circ$ at 3.3 m a.b). The fine-grained fraction in the bed sediment was set to 0.7% (due to bed armouring), in order to reproduce the order of magnitude of SSC profiles as suggested in the previous section (Fig. 9b). The coarser fractions were set to that of the bed sediment. Values of the depth-integrated suspended transports are reported in Table 4 for the fine ($<60\,\mu m$) and sand (all classes $>60\,\mu m$) fractions.

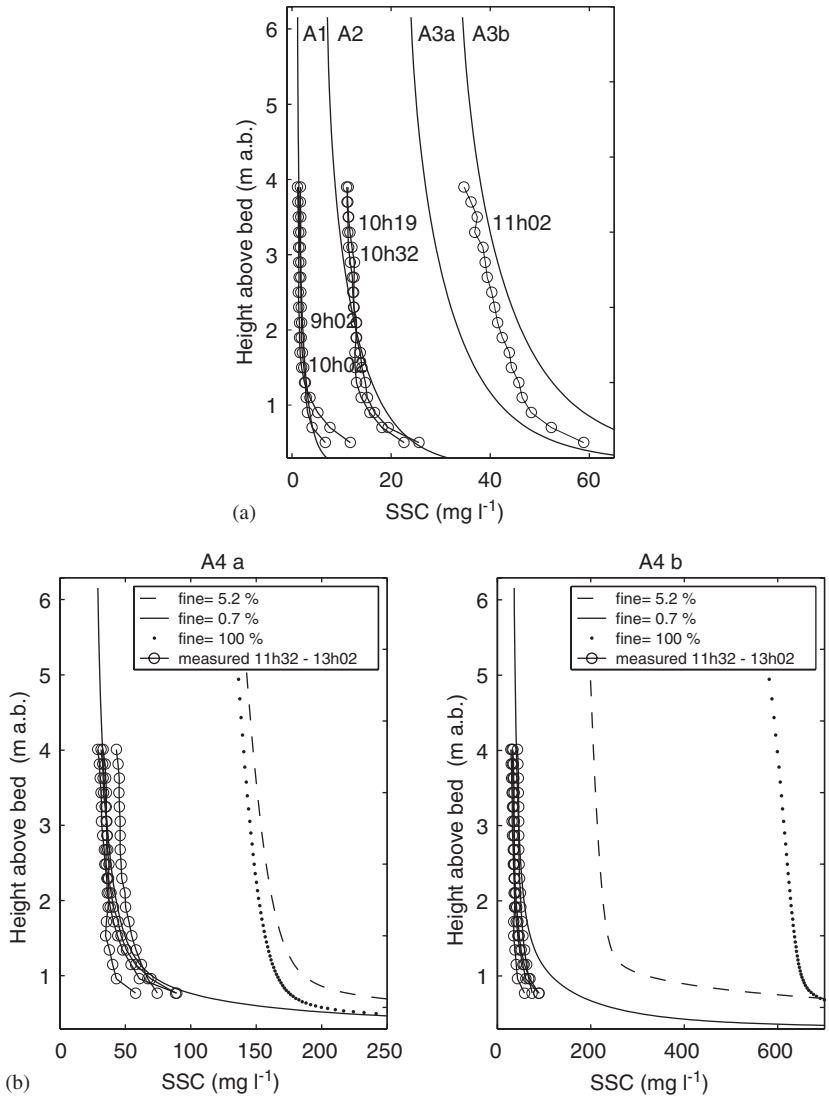

Fig. 9. (a) Computed (solid line) and measured (circle) SSC profiles, during the onset of storm between 8 h 50 min and 11 h on November 12th, 1999. Computations are plotted only for the fine-grained fraction representative of the study area (Table 1) and for hydrodynamic conditions A1–A3 as given in Table 3. (b) Computed SSC profiles for hydrodynamic corresponding to the average characteristics of the storm (A4ab, in Table 3) and for various silt and clay fractions of the bed: solid line (0.7%), dashed line (5.2%) and dotted line (100%). Empty circles represent the measured SSC profiles between 11 h 30 min and 13 h.

The computations agree (deviation of $\pm 11\%$), with the average suspended sediment flux measured between 0.9 and 4.1 m a.b during the storm ($104\,kg\,m^{-2}\,h^{-1}$). In addition, the computations indicate that the current-related transport dominates largely over the wave-related transport, unlike in the study of Storlazzi and Jaffe study (2002). This might be due to the strong current during the storm ($20–30\,cm\,s^{-1}$), but is also explained by the symmetry of the sine wave prescribed in our computations. Indeed, at our study site, free surface elevation records reveal irregular but quite symmetric waves, over the 26 m water depth. In contrast, in the Storlazzi and Jaffe study (2002), waves were clearly asymmetric under shallow water conditions (12 m depth) and, consequently, induced a strong wave-related transport.

The computations indicate also that the fine-grained fraction transport, integrated between 0 and 4.1 m a.b., contributes to about 73% of the bottom layer suspended sediment flux (Table 4). Furthermore, it indicates that 43% of the fine-grained

Table 4
Computed net transport for average storm conditions ($T_m = 8.1$ s, $H_s = 5.8$ m, $U_c = 0.25\,m\,s^{-1}$) with bed sediment composition set equal to 0.7% for silts and clays, 10.9% for fine sand, 42.2% for medium sand and 46.2% for coarse sand

Sediment transport ($kg\,m^{-1}\,h^{-1}$)		Current-related, in current direction	Current-related, in wave direction	Wave-related, in current direction	Wave-related, in wave direction
Finest particles (0–60 μm)	0–0.9 m a.b.	86.3	6.3×10^{-4}	−0.014	0.44
	0.9–4.1 m a.b.	115.5	6.1×10^{-4}	-0.5×10^{-6}	−0.26
Sand (>60 μm)	0–0.9 m a.b.	74.5	2.9×10^{-3}	−0.46	5.2×10^{-3}
	0.9–4.1 m a.b.	0.37	2.6×10^{-6}	-6.4×10^{-9}	2.5×10^{-3}

suspended sediment flux in the 4.1 m a.b. occurs in the last 0.9 m above the seabed, whereas this layer concentrates 99% of the sandy sediment flux in 4.1 m a.b.

3.3.4. Cross-shore changes

Computations of fine-grained SSC along a cross-shore transect (see location of transect on Fig. 1b) was performed, to identify the changes associated with depth variations of the wave energy and the sediment texture. Sediment fine-grained fraction and D_{50} are plotted against depth along this transect, on Fig. 10a, together with wave orbital velocity variations and SSC at 1 and 2 m a.b. for the conditions at the beginning of storm (A3b, Fig. 10b) and for the storm average conditions (A4a, Fig. 10c). The sand-mud transition depth, observed around 25–35 m in the bay, is representative of the seaward grain size gradient on the inner shelf of the Gulf of Lion (Fig. 1). Computations show the effect, along this transect, of two competitive factors: the decrease in wave orbital velocity; and the increase of the fine-grained fraction in the sediment, with increasing depth. The computations suggest that fine particle from muddy zones deeper than 35 m were not resuspended, during most part of the storm. SSC computations along a cross-shore transect indicate that this storm event resuspended sediment up to 35 m depth, suggesting that the seaward transition from sand to mud on the Gulf of Lion inner-shelf, outside the river prodeltas, may be controlled by the quasi-annual strong storms events.

Other authors have identified sediment resuspension down to 60 m depth, in the very fine-grained sediment of the Ebro shelf during a stronger storm event (i.e. $H_s > 4.5$ m, $T_s > 11$ s) (Puig et al., 2001; Palanques et al., 2002), even though they found a lag of 8 h between the peak of the storm and the increase of SSC. This lag was attributed, by the authors, to measuring conditions (5 m a.b.) and the time required to initiate sediment resuspension. This latter sets of data, concerning Mediterranean storms, indicates that for extreme storm conditions, sediment resuspension may reach the mid-shelf area.

4. Conclusion

This study emphasizes the key role of south-easterly swell, together with the low impact of predominant northwesterly continental winds, on coastal sediment resuspension in the Gulf of Lion. The storm observed in the Bay of Banyuls, in November 1999 and with the maximum significant wave height reaching 7 m and mean wave period of 10 s, is considered as a strong event that occurs once every 1 or 2 years. This event induced a strong turbidity increase throughout the water column. During the storm, SSC variations over a sandy bed at 26.3 m depth indicated a tenfold increase in the particle concentration, from 7 to $70\,mg\,l^{-1}$ at 0.5 m a.b and from 2–3 to $25\,mg\,l^{-1}$ at 4.1 m a.b. The increase of turbidity (level higher than the mean concentration before the storm) lasted for more than 8 days after the storm.

Computations of SSC profiles, with a 1DV RANS wave boundary layer numerical model, are in very good agreement with observed SSC; they indicate that the SSC during the first 2 h of the storm results from the suspension of the fine fraction (<60 μm) of the local sediment. After 2 h, the SSC computations suggest that winnowing of the fine particles, by the strong current, occurs together with bed armouring. Subsequently, the 1DV approach is no longer valid, as advection and exchange with adjacent zones are likely to occur. Temporal changes in the seabed grain-size distribution indicate the presence of an ephemeral fine-grained (~10 μm) superficial deposit after the storm; this lasted for 2 weeks in the study site. Moreover, computations of the mud fraction SSC, along a

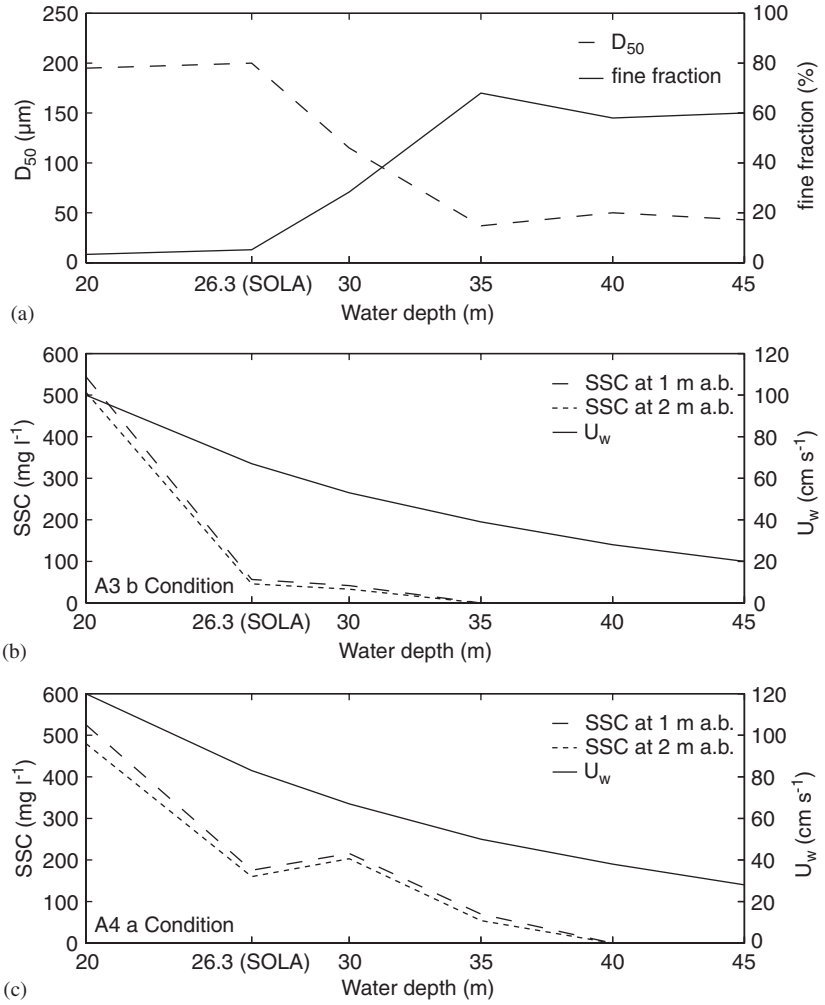

Fig. 10. Computed SSC produced by local resuspension at 2 m a.b. and 1 m a.b., wave orbital velocity, median grain size and fine-grained sediment ($<60\,\mu m$) fraction versus depth, along a cross-shore transect for A3 and A4 hydrodynamic conditions (see Table 3). Note that the SSC were computed using the fine-grained sediment fraction prior to the storm, although it is expected to decrease for the A4 condition, due to winnowing and bed armouring.

cross-shore transect, indicate that resuspension occurred for water depths shallower than 35 m. Thus, strong storm events that occur every 1 or 2 years could control the transition from sand to mud, which is located around 30 m.

Computed and measured suspended sediment fluxes indicate that large amounts of fine-grained particles are transported within the bottom boundary layer and throughout the water column, during the storm. This observation suggests that instruments profiling the whole of the water column, for current and SSC, are necessary to provide a better estimate of fine-grained sediment transport levels and fluxes, during storms. Therefore, ADCPs, that allow the simultaneous derivation of both parameters appear as an attractive alternative.

Acknowledgements

The authors acknowledge the support from the "Action de Recherche Thématique" no. 1 of the French "Programme National Environnement Côtier" and the European Commission under contracts MAS3–CTP96–0049 and EVK3–CT–2000–00023. L. Zudaire, the crew of the R/V Nereis II and the technical staff of the Laboratoire d'Océanographie Biologique de Banyuls-sur-Mer are thanked for the work at sea and the laboratory analysis. We thank

S.E. Poulos and P Traykovsky for their valuable reviews. We acknowledge the helpful comments and suggestions by D.M. Hanes on an earlier version of the manuscript.

References

Chang, G.C., Dickey, T.D., 2001. Sediment resuspension over a continental shelf during Hurricanes Edouard and Hortense. Journal of Geophysical Research 105 (C5), 9517–9531.

Drake, D.E., Cacchione, D.A., 1989. Estimates of the suspended sediment reference concentration (C_a) and resuspension coefficient (γ_0) from near-bottom observations on the California shelf. Continental Shelf Research 9, 51–64.

Durrieu de Madron, X., Ferré, B., Le Corre, G., Grenz, C., Conan, P., Pujo-Pay, M., Buscail, R., Bodiot, O. Trawling-induced resuspension and dispersal of muddy sediments and dissolved elements in the Gulf of Lion (NW Mediterrenean). Continental Shelf Research, this issue.

Engelund, F., Fredsøe, J., 1976. A sediment transport model for straight alluvial channel. Nordic Hydrology 7, 293–306.

Gardner, W., Blakey, J.C., Walsh, I.D., Richardson, M.J., Pegau, S., Zaneveld, J.R.V., Roesler, C., Gregg, M.C., MacKinnon, J.A., Sosik, H.M., Williams III, A.J., 2001. Optics, particles, stratification, and storms on the New England continental shelf. Journal of Geophysical Research 106 (5), 9473–9497.

Gibbs, R.J., 1985. Estuarine Flocs: their size, settling velocity and density. Journal of Geophysical Research 90 (C2), 3249–3251.

Grémare, A., Amouroux, J.M., Cauwet, G., Charles, F., Courties, C., deBovée, F., Dinet, A., Devenon, J.L., Durrieu de Madron, X., Ferré, B., Fraunié, P., Joux, F., Lantoine, F., Lebaron, P., Naudin, J.J., Palanques, A., Pujo-Pay, M., Zudaire, L., 2003. The effects of a strong winter storm on physical and biological variables at a shelf site in the Mediterranean. Oceanologica Acta 26 (4), 407–419.

Guillén, J., Palanques, A., Puig, P., Durrieu de Madron, X., Nyffeler, F., 2000. Field calibration of optical sensors for measuring suspended sediment concentration in the western Mediterranean. Scientia Marina 64 (4), 427–435.

Guillén, J., Jiménez, J.A., Palanques, A., Gracia, V., Puig, P., Sánchez-Arcilla, A., 2002. Sediment resuspension across a microtidal, low-energy inner shelf. Continental Shelf Research 22 (2), 305–325.

Guizien, K., Dohmen-Janssen, C.M., Vittori, G., 2003. 1DV bottom boundary layer modeling under combined wave and current: turbulent separation and phase lag effects. Journal of Geophysical Research 108 (C1), 3016.

Jago, C.F., Barusseau, J.P., 1981. Sediment entrainment on a wave-graded shelf, Roussillon, France. Marine Geology 42 (1–4), 279–299.

Land, J.M., Bray, R.N., 2000. Acoustic measurement of suspended solids for monitoring of dredging and dredged material disposal. Journal of Dredging Engineering 2 (3), 1–17.

Lee, G.H., Friedrichs, C.T., Vincent, C.E., 2002. Examination of diffusion versus advection dominated sediment suspension on the inner-shelf under storm and swell conditions, Duck, North Carolina. Journal of Geophysical Research 107 (C7), 3084.

Lyne, V.D., Butman, B., Grant, W.D., 1990. Sediment movement along the US East coast continental shelf, II. Modelling suspended sediment concentration during storms. Continental Shelf Research 10, 429–460.

Madsen, O.S., Chisholm, T.A., Wright, L.D., 1994. Suspended sediment transport in inner shelf waters during extreme storms. In: Proceedings of the 24th International Conference on Coastal Engineering, Barcelona, Spain, American Society of Civil Engineers, pp. 1849–1864.

Palanques, A., Puig, P., Guillén, J., Jiménez, J., Gracia, V., Sánchez-Arcilla, A., Madsen, O., 2002. Near-bottom suspended sediment fluxes on the microtidal low-energy Ebro continental shelf (NW Mediterranean). Continental Shelf Research 22 (2), 285–303.

Puig, P., Palanques, A., Guillén, J., 2001. Near-bottom suspended sediment variability caused by storms and near-inertial waves on the Ebro mid continental shelf (NW Mediterranean). Marine Geology 178, 81–93.

Shi, N.C., Larsen, L.H., Downing, J.P., 1985. Predicting suspended sediment concentration on continental shelves. Marine Geology 62 (3–4), 255–275.

Storlazzi, C.D., Jaffe, B.E., 2002. Flow and sediment suspension events on the inner shelf of central California. Marine Geology 181, 195–213.

Wiberg, P.L., Drake, D.E., Cacchione, D.A., 1994. Sediment resuspension and bed-armoring during high bottom stress events on the northern California inner continental shelf: measurements and predictions. Continental Shelf Research 14, 1191–1220.

Wilcox, D.C., 1992. The remarkable ability of turbulence model equations to describe transition, presented at Fifth Symposium on Numerical and Physical aspects of Aerodynamical Flows, 13–15 January, California State University, Long Beach, CA

Wright, L.D., Kim, S.-C., Friedrichs, C.T., 1999. Across-shelf variations in bed roughness, bed stress and sediment suspension on the northern California shelf. Marine Geology 154, 99–115.

Zanke, U., 1977. Berechnung der Sinkgeschwindigkeiten von Sedimenten. Mitteilungen des Franzius-Institutes 46, 231–245.